

Epitaxial TbMnO₃ thin films on SrTiO₃ substrates: A structural study

C.J.M. Daumont¹, D. Mannix², Sriram Venkatesan¹, G. Catalan³,
D. Rubi¹, B.J. Kooi¹, J.Th.M. De Hosson¹, B. Noheda¹

¹*Zernike Institute for Advanced Materials, University of Groningen, 9747 AG Groningen, The Netherlands*

²*Institut Néel, CNRS-UJF, 25 Avenue des Martyrs, 38042 Grenoble Cedex 9, France and*

³*Earth Science Department, Cambridge University, Cambridge CB2 3EQ, United Kingdom*

TbMnO₃ films have been grown under compressive strain on (001)-oriented SrTiO₃ crystals. They have an orthorhombic structure and display the (001) orientation. With increasing thickness, the structure evolves from a more symmetric (tetragonal) to a less symmetric (bulk-like orthorhombic) structure, while keeping constant the in-plane compression thereby leaving the out-of-plane lattice spacing unchanged. The domain microstructure of the films is also revealed, showing an increasing number of orthorhombic domains as the thickness is decreased: we directly observe ferroelastic domains as narrow as 4nm. The high density of domain walls may explain the induced ferromagnetism observed in the films, while both the decreased anisotropy and the small size of the domains could account for the absence of a ferroelectric spin spiral phase.

PACS numbers: 68.55.-a

I. INTRODUCTION

Multiferroics are a class of materials exhibiting coexistence of two or more ferroic orders[1, 2, 3, 4, 5]: (Anti-)ferromagnetism, (anti-)ferroelectricity, ferroelasticity and/or ferrotoroidicity. Multiferroic materials have been increasingly studied in recent years due to the possibility of substantial coupling between the ferroic properties within a single phase. The most interesting case for applications occurs when the magnetic and electric degrees of freedom are coupled, giving rise to a large magnetoelectric (ME) effect. This can eventually lead to a range of novel devices that use the control of the spontaneous magnetization (polarization) of a material with an electric (magnetic) field. Unfortunately, multiferroics are very rare and efforts have been made to discover and synthesize new multiferroic and magnetoelectric materials, as well as to understand the underlying mechanisms.

Among the possible mechanisms producing multiferroicity and large magnetoelectric coupling in single phase materials, the induction of ferroelectricity in spiral spin systems has been intensively studied[6, 7]. The orthorhombic perovskite TbMnO₃ is the best known example of such a system[4, 5, 8] and has also been shown to present giant ME effect[8]. Among the rare earth manganites, TbMnO₃ presents an intermediate Mn-O-Mn bond angle and lies, in the temperature versus ionic radius phase diagram, in between two different magnetic phases, displaying a complex magnetic behavior[9]. TbMnO₃ shows antiferromagnetic ordering below $T_N \sim 40\text{K}$, where the Mn spins align in an incommensurate sinusoidal structure. By decreasing the temperature further, the propagation vector of the sinusoidal spin structure decreases until it locks at $T_{lock} \sim 28\text{K}$, where the magnetic structure changes into a spiral structure[5, 8, 9, 10] that propagates along the b-axis. Due to the Dzyaloshinsky-Moriya(DM) interaction[11, 12], a spontaneous polarization along the c-axis and a strong ME effect arises below T_{lock} .

For practical devices, multiferroics are often preferred in thin film form. Moreover, the strain induced by the mismatch between the film and the substrate lattice parameters can lead to improving the materials properties with respect to the bulk. Interestingly, although TbMnO₃ is by now a very well known material, only a few reports on this perovskite in thin film form are available[13, 14, 15]. Since the magnetic and ferroelectric phases are determined by the crystal structure, a thorough characterization of the structure of the films is needed. This, however, is not straight forward due to the small thickness of the films and grazing incidence diffraction, using synchrotron sources, is required. In this work, we present the growth and structural characterization of TbMnO₃ perovskite thin films with thicknesses lower than 100nm on single crystals of (001)-SrTiO₃. (001)-SrTiO₃ is preferred in studies of epitaxy in perovskites because it can be obtained with atomically flat surfaces, favoring high quality growth. The films are shown to be very flat, c-oriented and epitaxially strained. Their unit cell is orthorhombic with an orthorhombic distortion that can be tuned with the film thickness up to a thickness of about 50nm.

Although ferroelectric and magnetoelectric measurements are still in progress, the magnetic properties (reported elsewhere[14]) suggest that these films are remarkably different from the bulk material: No evidence of the spiral spin structure that gives rise to multiferroic behavior was found in the magnetic data. On the other hand, ferromagnetic interactions are induced in the films, which renders them appealing for applications such as spin valves, where ferromagnetic insulators are required. This is in agreement with a very recent work on the same system[15] and reports in other orthorhombic manganite films[16]. We show here that the structure of the films and microstructure are likely to explain the difference between the films and bulk behavior.

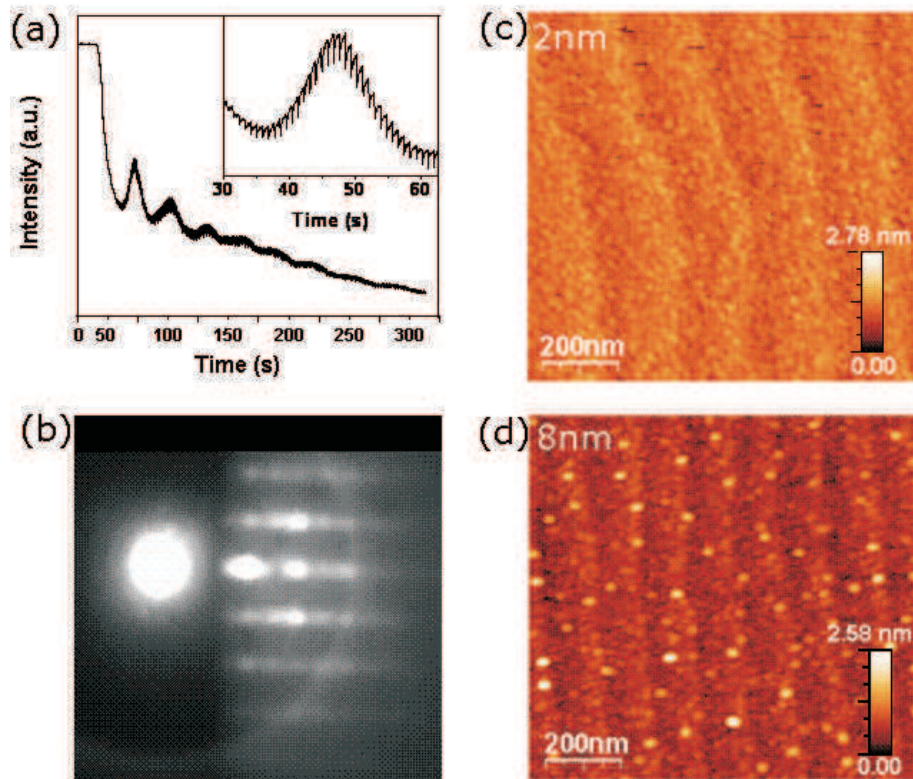


FIG. 1: (Color Online): (a) Intensity of the specular spot of the RHEED pattern as a function of deposition time. The inset is a blow-up of the first RHEED oscillation showing the laser pulses. (b) Typical RHEED pattern obtained after growth and annealing. The picture is taken after cooling down to room temperature and under vacuum. (c) and (d) AFM images of an 2nm and 8nm thin film, respectively, grown at $p_{O_2} = 0.25$ mbar. The vertical and horizontal scales are shown at the bottom of the pictures

II. EXPERIMENTAL

(001)-oriented $TbMnO_3$ (TMO) thin films were deposited on (001)- $SrTiO_3$ (STO) substrates by Pulsed Laser Deposition (PLD) assisted by reflective high energy electron diffraction (RHEED), using a KrF excimer laser with $\lambda = 248nm$. A stoichiometric target of $TbMnO_3$ was prepared by means of a standard solid-state reaction. Prior to deposition, the substrates were chemically treated and fired in O_2 in order to obtain TiO_2 single-terminated flat terraces [17]. The deposition of the films reported here was performed at $750^\circ C$ in oxygen pressures of 0.25 mbar to 0.9 mbar. The laser fluence was $2 J/cm^2$, with a repetition rate of 1Hz, and a distance between substrate and target of 55mm. After deposition, the films were slowly cooled down ($-3^\circ C/min$) to room temperature under an oxygen pressure of 100 mbar.

The highly distorted perovskite TMO crystallizes in a orthorhombic structure (space group: $Pbnm$) with lattice constants of $a_o = 5.2931 \text{ \AA}$, $b_o = 5.8384 \text{ \AA}$ and $c_o = 7.4025 \text{ \AA}$ [18]. However, lattice parameters reported so far for the bulk/single crystal system, and in particular the c -lattice parameter, vary significantly and this has been attributed to different growth conditions [6, 19, 20]. The STO substrate is a cubic perovskite with lattice constant of $a = 3.905 \text{ \AA}$. During growth, the intensities of the RHEED patterns change as a result of the relative surface coverage, roughening and disorder of the growing layers [21]. The intensity of the specular spot of the RHEED pattern was recorded from the beginning of the growth (see Figure 1(a)). With the first laser pulses, a large drop of the RHEED intensity takes place, indicating an important roughening of the surface with respect to the STO substrate. The recovery of intensity observed after approximately 35 laser pulses corresponds to the growth of the first complete layer of TMO.

The crystallinity and structure of the films were studied by standard x-ray diffraction (XRD) with a Panalytical X'Pert MRD diffractometer, while their surface morphology was probed by means of a Nanoscope IIIa atomic force microscope (AFM). X-ray photoelectron spectroscopy (XPS) experiments were performed in a SSX-100 spectrometer from Surface Science Instruments with a monochromatic Al-K x-ray source ($h\nu = 1486.6eV$). XPS in films of different thickness and grown at different oxygen pressures are consistent with a manganese valence of +3 and no evidence of

Mn⁴⁺ or Mn²⁺ was found [14]. In order to probe the in-plane lattice, grazing incidence x-ray diffraction (GIXD) was performed with synchrotron radiation, both at the W1 beamline in HASYLAB-DESY (Hamburg) and the XMaS beamline in ESRF (Grenoble). TEM plan-view specimens were prepared by conventional procedure involving cutting, grinding, polishing, dimpling and ion milling. A precision ion polishing system (Gatan model 491) with 4 Kv Ar⁺ beams was used, in which both guns make an angle of 8° with the bottom side of the substrate. On the other side, the film is covered with a piece of glass to avoid any contamination by redeposition from the sputtered backside. The observations have been performed with a JEOL 2010F electron microscope at an accelerating voltage of 200 kV.

III. RESULTS

About eight RHEED intensity oscillations can be seen at the beginning of the growth corresponding to an initial layer-by-layer (2D-like) growth. However, those oscillations are superimposed on a decreasing intensity background, indicating that an overall roughening occurs as the growth proceeds. After the oscillations have faded away and the intensity of the specular spot has decreased to a certain intensity, the later remains constant during the rest of the deposition (outside of the graph range) and the pattern changes from a purely stripy pattern to the mixed stripe-spot pattern shown in Figure 1(b). This type of behavior has been reported recently for other oxides as a 'pseudo-2D islands growth'[22, 23]. This change from 2D character to 'pseudo'-3D character of the growth has also been identified using AFM. Indeed, Figure 1(c) shows the morphology of a 2nm film, for which the deposition was stopped shortly before the 2D-to-3D transition. It can be seen that the film is atomically flat, showing the step-and-terrace morphology of the substrate. However, when the deposition is stopped at the initial stage of the transition from 2D to 3D growth, particles with a diameter of around 30 nm start appearing, as shown in Figure 1(d). We found that the change from 2D to 3D growth occurs at a thickness in between 2 and 5 nm.

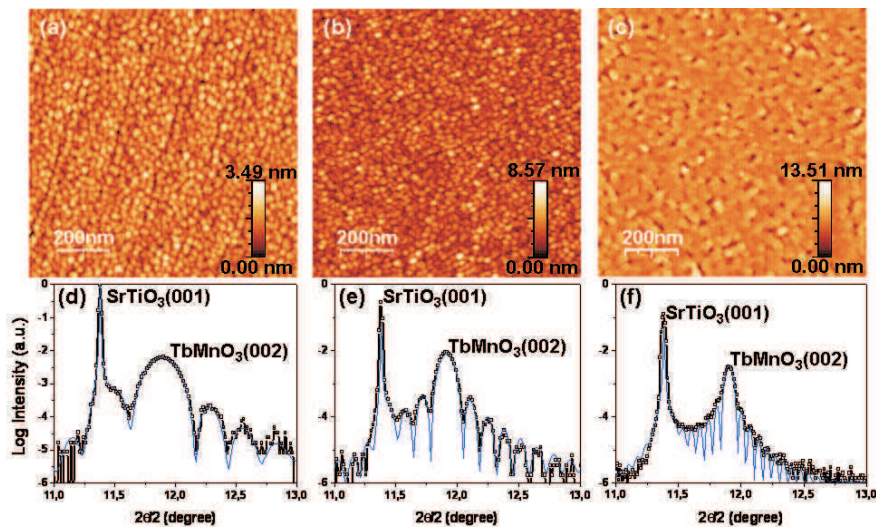


FIG. 2: (Color Online): AFM images of 17nm (a), 34nm (b) and 67nm (c) thick TMO thin films grown with a $pO_2 = 0.25$ mbar. The scans area is $1\mu m \times 1\mu m$. The corresponding diffraction patterns can be seen in (d), (e) and (f), respectively. The experimental data are shown as thick black lines. The fit to the data is shown in each case as a thin blue line.

Figures 2(a) to 2(c) show AFM images of three TMO films with different thicknesses grown under the same conditions. In the 17nm film (Figure 2(a)), although it is already in the 3D growth regime and the grains dominate the film morphology, the steps from the substrate are still visible. The steps are not clearly visible for a 34nm film and a 67 nm (Figures 2(b),(c)). Figures 2(d)-(f) show typical 2θ - ω x-ray diffractograms around the (001)_c Bragg reflection of STO (the most intense ones in the pattern), for the same three films. The film peaks are those at the right hand-side of the STO reflections. The blue lines are the fits of the crystal truncation rod using a kinematical model. These calculations take into account, not only the complex refractive index of the substrate and the film, but also the angular dependent atomic scattering factors. The high quality and flatness of the interfaces is evidenced by the Laue fringes around the film peak for thicknesses up to 67nm.

Figure 3 shows a broader 2θ - ω scan including both the (001)_c and the (002)_c STO Bragg reflections. No secondary or impurity phases could be observed. A phi-scan around the (024)_{pc} (ie $(2\bar{2}8)_o$) of TMO (see inset) shows the peaks separated 90 degrees from each other, confirming the four-fold symmetry of the film and the coherent growth. From

the position of the film peaks of figure 3, an out-of-plane lattice spacing of 3.737 Å was found. X-ray diffraction, thus, shows that the films are single phase and (001)-oriented (with the c -axis perpendicular to the surface). Using a value of Poisson ratio of 0.35, typical in manganites[24], the out-of-plane lattice spacing is estimated to expand from 3.70 Å ($c/2$ of bulk TMO) to about 3.74 Å, in good agreement with our measurements.

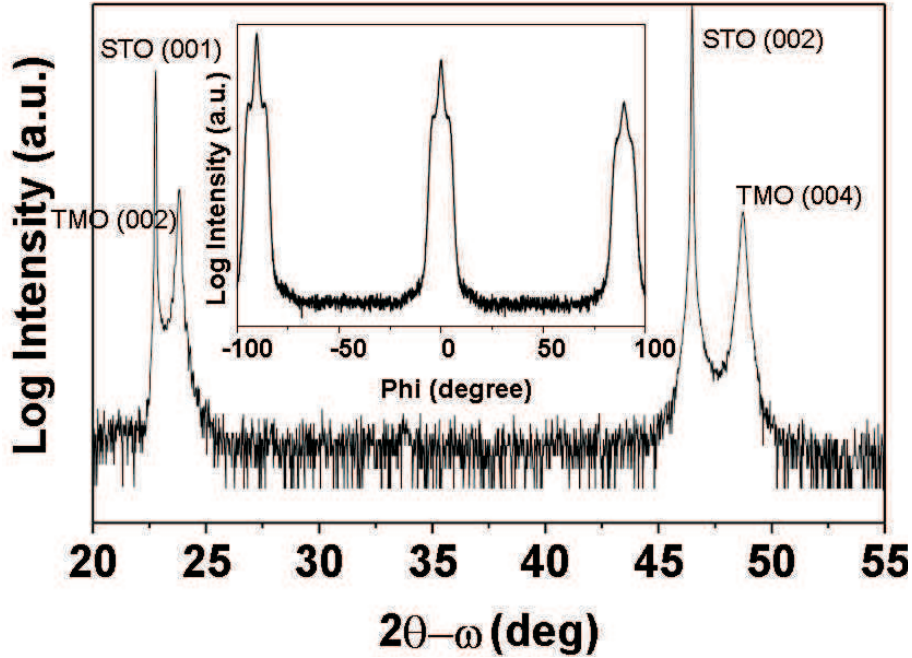


FIG. 3: 2θ - ω for a 67nm thick film of TMO grown on STO. Inset: Phi-scan around the $(2\bar{2}8)_o$ reflection.

A larger out-of-plane lattice parameter than the bulk's one could also be explained by a film whose strain is relaxed by means of oxygen vacancies, as they are known to expand the unit cell[25, 26]. To investigate this possibility, the oxygen pressure during deposition was increased up to 0.9 mbar (the maximum attained in our set-up). Within the range of oxygen pressure investigated, the out-of-plane lattice parameter indeed decreases linearly with increasing oxygen pressure during deposition, consistent with the number of oxygen vacancies decreasing for increasing pressures. The maximum pressure of 0.9 mbar seems to be large enough to produce stoichiometric films since the unit cell of the relaxed layers is as large as the bulk's one, as it will be discussed later.

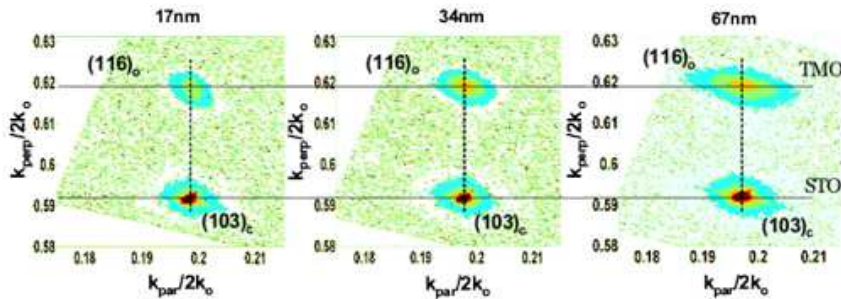


FIG. 4: (Color Online): Reciprocal space maps around the $(103)_c$ Bragg reflection of the STO substrate for 17nm, 34nm and 67nm films grown at 0.25 mbar. The vertical and horizontal lines are guides to the eyes. The abscissa (ordinate) represents the in-plane (out-of-plane) component of the scattering vector. Both are normalized by $2k_o=4\pi/\lambda$.

A detailed investigation of the film structure was performed using x-ray diffraction to map selected areas of the reciprocal space. Figures 4(a)-(c) show reciprocal space maps (RSMs) around the $(103)_c$ Bragg reflections of a 17nm, 34nm and 67nm thick film, respectively, grown at 0.25mbar. The peaks corresponding to the films (substrates) are those at larger (smaller) K_{perp} (see horizontal lines in the figure). The in-plane and out-of plane components of the $(103)_c$ and $(013)_c$ TMO peaks do not change as a function of thickness and the in-plane lattice parameter remains

identical to that of STO for thicknesses up to 67nm, indicating that the films are coherent with the substrate along the pseudo-cubic [100] or [010] directions. As the thickness is increased, only a broadening of the rocking curve of the TMO film can be seen, indicating increase of mosaicity. However, when the RSM is taken around the $(113)_c$, a different picture is observed, as shown in figure 5(a) for a 67nm thin film. Instead of a coherent film peak, two film peaks are found that could be indexed as orthorhombic $(206)_o$ and $(026)_o$. The data therefore, fit a structural model in which the films are orthorhombically distorted, similar to the bulk material, but keep coherence with the cubic substrate along the [100] or [010] directions.

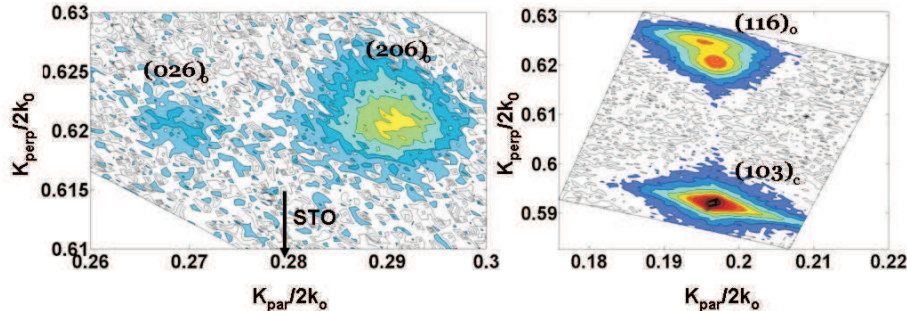


FIG. 5: (Color Online): (a) RSM around $(206)_o$ and $(026)_o$ for a 67nm thick TMO film grown at 0.25 mbar. The arrow indicates the k_{par} of the STO substrate. (b) RSM around the $(103)_c$ STO Bragg reflection for a 80nm thick TMO film grown at 0.9 mbar. The abscissa (ordinate) represents the in-plane (out-of-plane) component of the scattering vector, both normalized by $2k_o = 4\pi/\lambda$.

The orthorhombic a_o , b_o and c_o lattice parameters can be extracted from the $(116)_o$ and $(206)_o$ reflections shown above. Figure 6 shows the evolution of the lattice parameters as a function of thickness for the films grown with $pO_2 = 0.9$ mbar and $pO_2 = 0.25$ mbar. Both series display similar trend, showing that the oxygen vacancies, which are likely to be present in the films grown at the lowest pressure, giving rise to larger c_o values, do not change the general behavior. The orthorhombic distortion is the smallest for the thinnest films and a 2nm thick TMO film shows a tetragonal symmetry as evidenced by GIXD (not shown here). With increasing thickness, c_o remains unchanged, while a_o decreases and b_o increases towards their bulk value. However, the bulk lattice parameters are not reached in a continuous way and a_o and b_o saturate for a thickness of around 50 nm. Above about 70nm, a new spot appears in the diffraction maps, as shown in Figure 5(b). This second spot corresponds to a relaxed unit cell with bulk lattice parameters (dashed lines in Figure 6). The fact that, in the films grown at 0.9mbar, this spot appears with lattice parameters almost identical to the bulk ones, strongly indicates that these films are stoichiometric, as discussed above. We have shown that the films are orthorhombic but keep coherence with the cubic substrate along the $[010]_c$ or $[100]_c$ directions. Thus, the films orthorhombic lattice parameters fulfill $a_o^2 + b_o^2 = (2a_{STO})^2$ for all thickness and only the in-plane angle γ (see figure 9) changes with increasing thickness. Therefore, the strain state is constant and so is the c lattice parameter.

In order to better understand the in-plane coherence of the films with the substrate and the domain structure of the film, GIXD experiments were performed using synchrotron radiation. Figure 7 (a)-(d) shows in-plane RSM's around selected reciprocal lattice points of the STO lattice for a 8 nm thin film grown at 0.25mbar. In all the maps, the central sharp spot corresponds to the STO Bragg peak and the other broader visible reflections around it are from the TMO film. As shown in (a), four broad peaks can be seen around the (110) substrate spot. They correspond to the different equivalent orientations of the orthorhombic unit cell (see sketch in figure 9). The presence of these four domains maintains in the film the four-fold symmetry of the cubic substrate. Moreover, as shown in figure 7(b) and (c), a peak broadening in the perpendicular direction (along the $[010]$ for the (100) reflection and along $[100]$ for the (010) reflection), the so-called rocking curve, is seen around the central cubic position. This corresponds to the part of the film that is coherent with the substrate (with lattice spacing 3.90 Å). As seen in Figure 7(d), around the $(220)_c$, only two of the four peaks can be observed, those corresponding to the $(400)_o$ reflections. The absence of the $(040)_o$ peaks is due to the relative intensities of those reflections. Indeed, the intensity ratio $I(200)_o/I(020)_o$ is 1.4 in bulk, whereas a ratio of 77 is found for $I(400)_o/I(040)_o$. This makes the intensity of the $(040)_o$ too weak for us to detect it.

GIXD experiments were also performed for a 55nm film grown at 0.25mbar. Figure 8 (a)-(d) shows different in-plane RSMs for this thicker film. From (a), only two film reflections are observed around the substrate (110) peak (which in this case is not visible due to the grazing incidence geometry and the larger thickness of the film). The peaks correspond to the $(200)_o$ (higher H and K values) and the $(020)_o$ (at lower H and K values). Analysis of these diffraction maps indicates that, along with the change of a_o and b_o , a gradual rotation of the unit cell also occurs at larger thickness, so that the orthorhombic axes (a_o and b_o) align parallel to the $[110]$ of STO (see figure 9c). This can

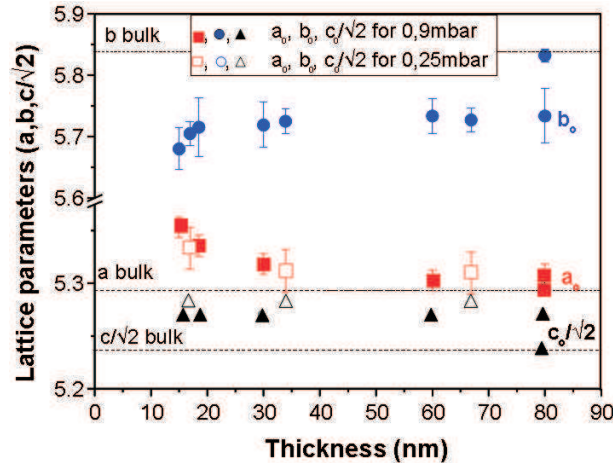


FIG. 6: Orthorhombic lattice parameters (a_o , b_o , $c_o/\sqrt{2}$) as a function of thickness for films grown with $pO_2=0.9$ mbar (filled symbols) and 0.25mbar (open symbols). In the 80nm film, two phases are found and one of them (symbols marked with a star) corresponds to the bulk orthorhombic unit cell[18]. The lines are guides to the eye.

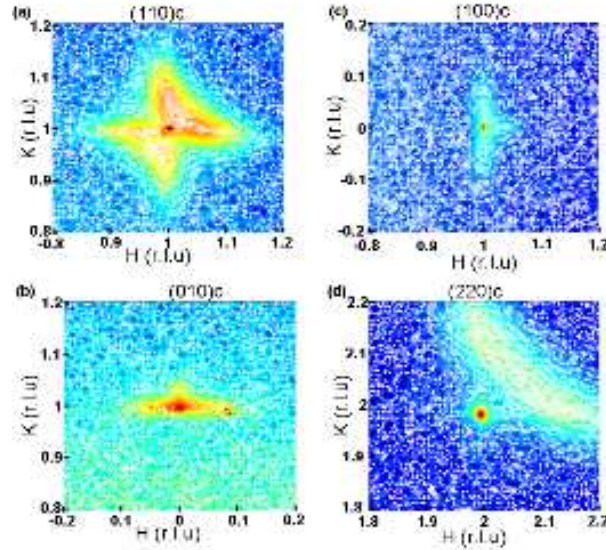


FIG. 7: (Color online): RSMs of a 8nm TMO film grown at 0.25mbar around: (a) the $(110)_c$; (b) the $(010)_c$; (c) the $(100)_c$ and (d) the $(220)_c$ STO Bragg reflections. The axes are in reciprocal lattice units of the substrate ($1 \text{ r.l.u.} = 2\pi/3.905 \text{ \AA}$)

be better seen in figures 8 (a) and (d), where the extremely broad peak is due to domains existing at all orientations in between those sketched in figure 9(a) and (b) and those in (c). The coherence with the substrate in the thinner films is then given by $[110]_o$ parallel to $[100]_c$ (or to $[010]_c$). By further increasing the thickness, the strain energy has increased such that the coherency along the $[100]_c$ cannot be kept and the films relax to their bulk structure, with the orthorhombic in-plane axis parallel to the $[110]$ of STO.

Figure 10 shows TEM plan view images and electron diffraction patterns recorded for two samples with thicknesses of 17nm and 67nm. In the plan view image of the 17nm TMO film, two differently oriented types of rectangular domains can be seen along with strain contrast for domains having the same orientation. This is consistent with the four types of domains seen via XRD. For the thicker film, two orientations can still be seen along with bigger domains, consistent with the coalescence of the grains seen by AFM. Moreover, strain contrast is present within the domains showing that the domains coalesce as the thickness increases. Screw dislocations can be seen on the thicker film. In addition of screw dislocations at the interface, another type of defects probably exist at the domain boundaries that take care of the in-plane rotation of the domains. The electron diffraction patterns confirm what has been seen in x-ray diffraction: for the thinner film, the diffraction peaks are the superposition of four TMO domains along with the contribution from the substrate; for the 67nm TMO thin film, the electron diffraction pattern differs from that of

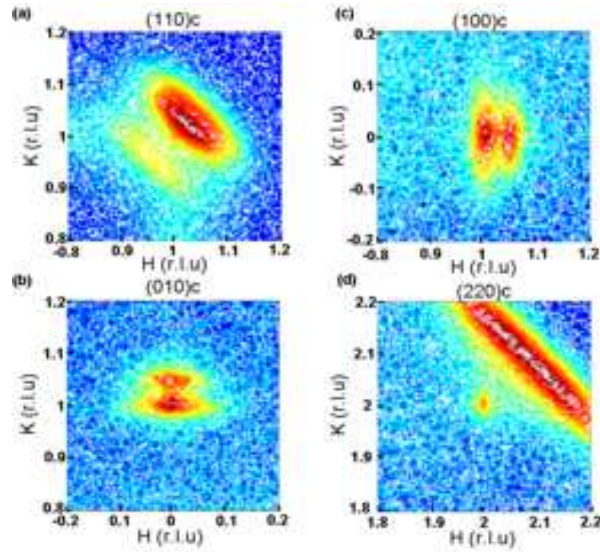


FIG. 8: (Color online): RSMs for a 55nm TMO film grown at 0.25mbar around (a) the $(110)_c$; (b) the $(010)_c$; (c) the $(100)_c$ and (d) the $(220)_c$ STO Bragg reflections. The axes are in reciprocal lattice units of the substrate ($1 \text{ r.l.u.} = 2\pi/3.905 \text{ \AA}$)

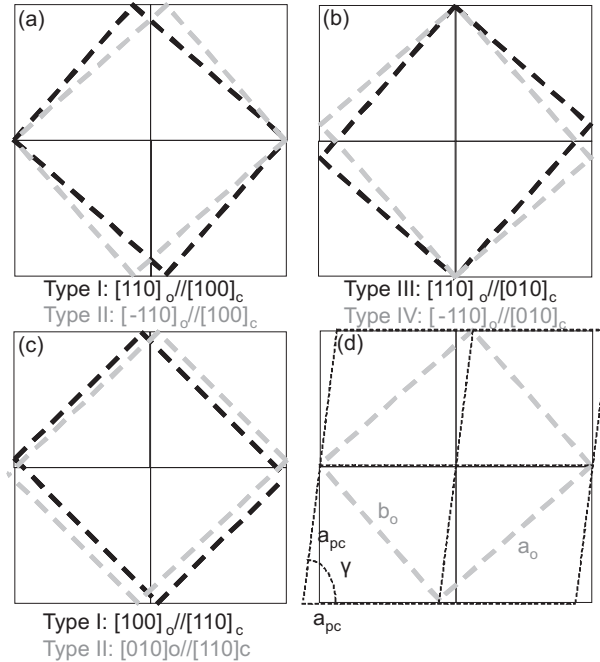


FIG. 9: (a) and (b) Sketch of the four types of orthorhombic domains present in the thinner films and their coherence with the substrate. (c) Sketch of the orthorhombic domains present in the thicker films and their coherence with the substrate. (d) Relationship between the orthorhombic and pseudo-cubic lattice parameters with the substrate lattice

the very thin films and shows a rotation gradient, as discussed above.

IV. DISCUSSION

For the 17nm film, the domains are found to have a small width of about 4nm (see Fig. 10a). This domain size is particularly small when compared with the typical thickness of magnetic domain walls, which are of the order of several nm[27, 28]. This means that in the thin films the fraction occupied by domain walls is comparable to that of the domains themselves, and therefore the properties of the domain walls are likely to affect the overall magnetic properties,

that is, the induced weak ferromagnetism, and perhaps even the absence of a lock-in transition[14]. For example, while the orthorhombic domains are known to be antiferromagnetic in character, in agreement with the negative Curie-Weiss temperature measured in the films[14], the magnetic interactions at the domain walls can give rise to a ferromagnetic component. Symmetry arguments show that magnetoelectric coupling can induce ferromagnetism in the domain walls of ferroelectric antiferromagnets[29], and works by Fiebig and co-workers have also shown that the ferroelectric domain walls of multiferroic hexagonal manganites can have a net magnetization at their center[30] as well as enhanced magnetoelectric coupling[31].

The small domain size is likely to also affect the spin spiral. In bulk TbMnO_3 , the period of the spiral is of the order of 2nm, which is comparable to the domain size and so it may well be destroyed by the proximity of the domain boundaries. Moreover, even if the spiral spin order that gives rise to the lock-in and ferroelectric transition survived, the domain size may be incommensurate with the spiral period, meaning that some spins will not be fully compensated, an effect that will be more noticeable for smaller domains. The presence of small domains would also prevent long range coherence, since the spiral propagation direction, which is along the orthorhombic b-axis, has to flick from x to y directions at each domain wall.

Finally, the reduction of in-plane anisotropy means that the difference between the a and b lattice parameters in the orthorhombic structure decreases. For the extreme case of the tetragonal films (2nm thick or less) there is no privileged direction, and hence there can be no spin spiral. But even for the thicker orthorhombic films, strain is likely to affect, or even destroy, the spin spiral, since the changes in in-plane anisotropy with respect to the bulk compound must also affect the Mn-O-Mn bond angle, which is known to be the critical parameter for the appearance of the lock-in spiral phase[32]

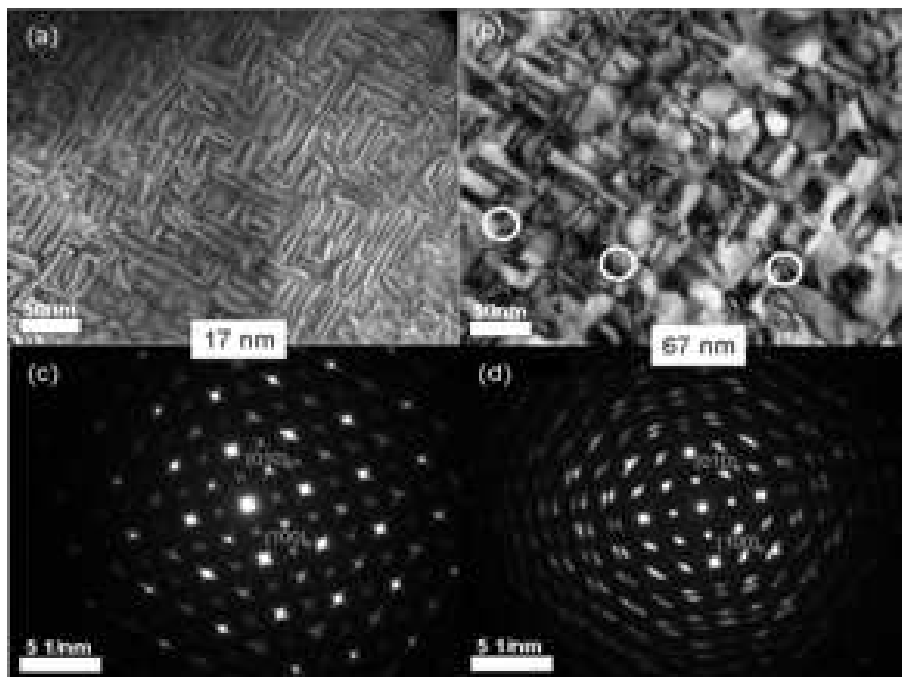


FIG. 10: Plan view TEM pictures of a 17nm (a) and 67nm (b)TMO film. Electron diffraction patterns of the same films are shown in (c) and (d), respectively. The white circles shows show the presence of dislocations.

V. CONCLUDING REMARKS

We have successfully deposited epitaxial orthorhombic TbMnO_3 films on (001)- SrTiO_3 , with thicknesses ranging from 8nm to 80nm. The crystal structure of the thin strained films has been identified as a less distorted orthorhombic unit cell compared to the bulk one with $a_{film} > a_{bulk}$, $b_{film} < b_{bulk}$ and $c_{film} > c_{bulk}$. We found that the films grow with the c-axis out of plane and they orient themselves in the plane such that the $\langle 110 \rangle_o$ directions align with the $\langle 100 \rangle_c$ directions of the substrate. The orthorhombic lattice parameters a_o and b_o are constraint by epitaxy so that $a_o^2 + b_o^2 = (2a_{STO})^2$. This allows for four equivalent orientations and, therefore, four types of domains are observed, such that the in-plane diffraction patterns display four-fold symmetry.

With increasing thickness, the in-plane orthorhombic axes gradually change towards their bulk values, increasing the orthorhombicity of the films, but still keeping the partial coherence and epitaxy relation $a_o^2 + b_o^2 = (2a_{STO})^2$. Due to this, the amount of in-plane compression (and hence out-of-plane elongation) remains unchanged up to thicknesses of about 70nm. Above this thickness, the lattice relaxes to the bulk one. In spite of the unchanged in-plane compression, the thicker films do show a distribution of unit cell rotations coupled with increasing orthorhombic distortion.

It has been shown[14] that the physical properties of these films are very different from those of the bulk: The films show ferromagnetic interactions and spin-glass-like behavior below the Néel temperature of $\sim 40K$, which are absent in the bulk. This can be of interest due to the scarcity of ferromagnetic insulators. Similar results have recently been obtained for this and other orthorhombic perovskites[15, 16]. Here, we propose that this is directly associated to the domain walls, showing evidence that these constitute a large part of the volume of the films. On the other hand, the magnetic anomaly observed in the bulk material at about 28K, related to the transition to the spiral spin structure and the onset of ferroelectricity, could not be observed in these films[14]. This may be due to the decrease of in-plane anisotropy that we show takes place with decreasing thickness, or to the small domain size. Work is in progress to investigate these possibilities.

VI. ACKNOWLEDGEMENTS

The authors would like to thank Umut Adem, Graeme Blake, Claire Colin, Maxim Mostovoy, Mufti Nandang, Gwilherm Nenert, Thom Palstra, Gijsbert Rispens, Oliver Seeck and Ard Vlooswijk for useful discussions and, very specially, Henk Bruinenberg, for his invaluable technical support. Finally, financial support by the EU STREP project MaCoMuFi(FP6-03321) is gratefully acknowledged.

VII. REFERENCES

-
- [1] N. A. Hill *et al.*, J. Phys. Chem. B **104**, 6694 (2000)
 - [2] M. Fiebig *et al.*, J. Phys. D. **38**, R123 (2005)
 - [3] W. Eerenstein *et al.*, Nature **442**, 759 (2006)
 - [4] Y. Tokura *et al.*, Science **312**, 1481 (2006)
 - [5] Y. Tokura *et al.*, Journ. Magn. Magn. Mat. **310**, 1145 (2007)
 - [6] M. Kenzelmann *et al.*, Phys. Rev. Lett. **95**, 087206 (2005)
 - [7] M. Mostovoy *et al.*, Phys. Rev. Lett. **96**, 067601 (2006)
 - [8] R. Kajimoto *et al.*, Phys Rev B **70**, 012401 (2004)
 - [9] T. Goto *et al.*, Phys. Rev. Lett. **92**, 257201 (2004)
 - [10] T. Kimura *et al.*, Nature **426**, 55 (2003)
 - [11] I. A. Sergienko *et al.*, Phys. Rev. B **73**, 094434 (2006)
 - [12] A. Malashevich *et al.*, Phys. Rev. Lett. **101**, 037210 (2008)
 - [13] Y. Cui *et al.*, Solid State Comm. **133**, 641 (2005)
 - [14] D. Rubi *et al.*, preprint available at: <http://arxiv.org/abs/0810.5137v1>.
 - [15] B.J. Kirby *et al.*, preprint available at: <http://arxiv.org/ftp/arxiv/papers/0811/0811.4430.pdf>
 - [16] X. Marti *et al.*, preprint available at: <http://arxiv.org/ftp/cond-mat/papers/0701/0701387.pdf>
 - [17] G. Koster *et al.*, **73**, 20, 2920 (1998)
 - [18] J.A. Alonso *et al.*, Inorg. Chem. **39**, 917 (2000)
 - [19] J. Blasco *et al.*, Phys. Rev. B **62**, 5609 (2000).
 - [20] N. Aliouane *et al.*, Phys. Rev. B **73**, 020102 (2006)
 - [21] A. Ichimiya and P. I. Cohen, Cambridge University Press: Cambridge, (2004)
 - [22] J. Shin *et al.*, Appl. Phys. Lett. **91**, 202901 (2007)
 - [23] B. Daudin *et al.*, Materials Science and Engineering B **50**, 8 (1997)
 - [24] L. Ranno *et al.*, Appl. Surf. Sci. **188**, 170 (2002)
 - [25] M. Babei and D. K. Ross, Physica C **425**, 130 (2005)
 - [26] D.A. Rudman *et al.*, Applied Superconductivity, **9**,2460 (1999)
 - [27] A. Hubert and R. Schäfer, Magnetic Domains 1998 (Berlin: Springer)
 - [28] G. Catalan *et al.*, J. Phys.: Condens. Matter **19**, 022201 (2007)
 - [29] J. Privratska and V. Janovec Ferroelectrics **204**, 321 (1997); Ferroelectrics **222**, 23 (1999)
 - [30] A.V. Goltsev *et al.*, Phys Rev Lett. **90**, 177204 (2003)
 - [31] T. Lottermoser and M. Fiebig, Phys Rev B **70**, 220407(R) (2004)

[32] T. Kimura *et al.*, Phys. Rev. B **68**, 060403(R) (2003)